Int. Journal of Refractory Metals and Hard Materials 52 (2015) 131–136

Contents lists available at ScienceDirect

Int. Journal of Refractory Metals and Hard Materials

journal homepage: www.elsevier.com/locate/IJRMHM

Preparation and ductile-to-brittle transition temperature of the La-TZM alloy plates

Ping Hu [a,*], Fan Yang [a], Kuai-She Wang [a], Zhi-tao Yu [a], Jiang-fei Tan [a], Rui Song [a], Bo-liang Hu [a], Hua Wang [b], Huan-Cheng He [a], Alex A. Volinsky [c]

[a] School of Metallurgy Engineering, Xi'an University of Architecture and Technology, Xi'an 710055, China
[b] Xi'an Electric Furnace Institute Co., Ltd., Xi'an 710061, China
[c] Department of Mechanical Engineering, University of South Florida, Tampa, FL 33620, USA

ARTICLE INFO

Article history:
Received 27 November 2014
Received in revised form 17 March 2015
Accepted 1 May 2015
Available online 5 May 2015

Keywords:
La doping
TZM alloy
La doping
Mechanical properties
DBTT

ABSTRACT

Powder metallurgy methods were utilized to prepare lanthanum-doped titanium–zirconium–molybdenum (La-TZM) and traditional TZM alloy plates. Tensile and Charpy impact tests were employed to study the room temperature and cryogenic mechanical properties of the two kinds of TZM alloys. For the same process conditions, the lanthanum doping has significantly improved the tensile strength and elongation, which increased by 28.2% and 32.8%, respectively. For these process conditions, the La-TZM has higher density and smaller evenly distributed secondary phases. Compared with TZM, the secondary phase in La-TZM is finer, and hinders the spreading of cracks. This is why the La-TZM alloy plates have higher strength and elongation. By doping lanthanum, the ductile-to-brittle transition temperature of the TZM alloy decreased from −80 °C to −120 °C. The secondary phase La particles refine the grain and hinder fracture expansion across the grains during the impact fracture of the La-TZM alloy. TZM alloy improved room temperature and cryogenic mechanical properties significantly expand its application range.

1. Introduction

TZM alloy contains 0.5–0.8 wt.% titanium, 0.08–0.1 wt.% zirconium, 0.016–0.02 wt.% carbon and molybdenum balance. Molybdenum TZM alloys are highly desirable for a wide range of critical applications due to their high electrical and thermal conductivity, strength and creep resistance at elevated temperatures, high temperature stability, low coefficient of thermal expansion and excellent corrosion resistance in liquid metals [1–7]. They are widely used in aerospace, power generation, nuclear and fusion reactors, and military, industrial and chemical applications, where these alloys are subjected to high temperatures, liquid metal corrosion and other aggressive environments [8].

However, TZM alloy is brittle at room temperature and has a high ductile-to-brittle transition temperature (DBTT), which is not desirable for manufacturing and applications [9–11], also limited by the poor high temperature oxidation resistance. To expand the scope of applications, many studies were conducted to improve the mechanical properties and high temperature oxidation resistance.

The ductile-to-brittle transition temperature of a metal represents the point at which the fracture energy reduces below a predetermined point. DBTT is important, since once a material is cooled below the DBTT, it has a much greater tendency to shatter on impact instead of deforming plastically. DBTT is a very important consideration in material selection when the material in question is subject to high mechanical stresses. The most accurate method of measuring the ductile-to-brittle transition temperature of a material is by fracture testing, such as the Charpy impact testing and four-point bend testing [12].

Previous studies have shown that doping La_2O_3 into traditional TZM alloy can significantly improve its strength and toughness [9,13]. Effects of lanthanum doping on the oxidation behavior of TZM alloys have been previously researched by this group [8]. This article investigates the effect of lanthanum doping on the mechanical properties and the DBTT of TZM alloy plates.

Table 1
Composition of the TZM alloys (wt%).

Sample	Ti	Zr	Stearic acid	$La(NO_3)_3$	Mo
#1	0.5	0.1	0.25	1.99	Balance
#2	0.5	0.1	0.25	0	Balance

* Corresponding author.
E-mail address: huping1985@126.com (P. Hu).

http://dx.doi.org/10.1016/j.ijrmhm.2015.05.006
0263-4368/

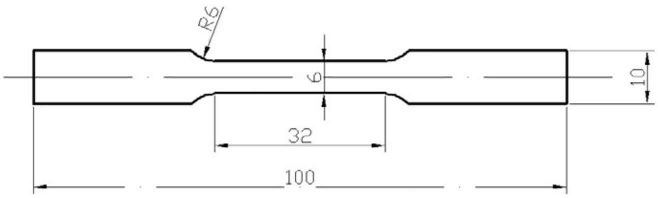

Fig. 1. The tensile specimen geometry of the La-TZM and TZM alloy plates. Dimensions are given in mm.

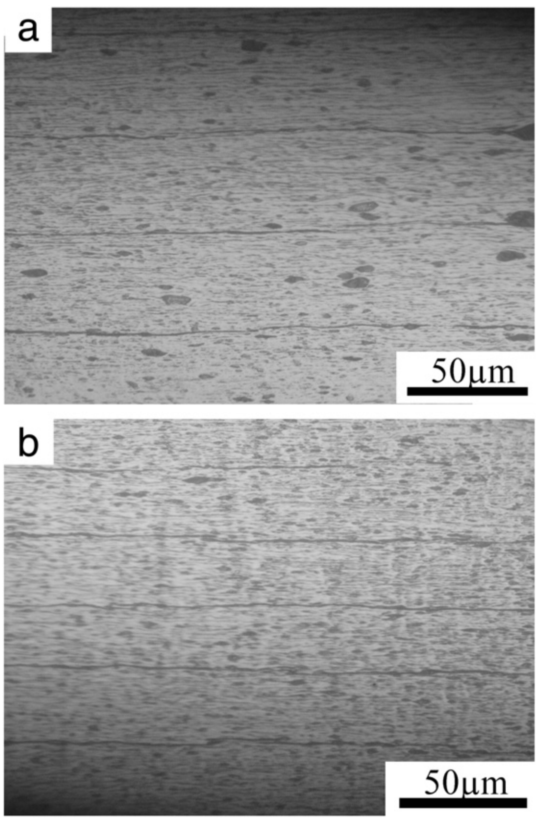

Fig. 2. Optical images of the cross-sectional microstructure of (a) TZM alloy and (b) La-TZM alloy plates.

Table 2
The tensile test data of the La-TZM and TZM alloys.

Sample	TZM	La-TZM	Average growth rate (%)
Strength (MPa)	1096 ± 20	1405 ± 20	28.2
Elongation (%)	7.0 ± 0.5	9.3 ± 0.5	32.8

2. Experimental procedure

2.1. Preparation of TZM and La-TZM alloys

Based on the design composition, listed in Table 1, two kinds of TZM alloys were prepared: La-doped TZM alloy (#1) and traditional TZM alloy (#2). Both kinds of alloys were manufactured into two plates, 0.5 mm and 10 mm thick. The preparation of the 0.5 mm thick TZM and La-TZM alloy plates is described in a previous publication [8]. The preparation of the 10 mm thick plates is also described in reference [8], except for the last processing step of warm rolling.

2.2. Tensile testing

The tensile specimens were made from the 0.5 mm thick rolled alloy plates and the geometry is shown in Fig. 1. The tensile tests were conducted using the 5 kN hydraulic universal testing machine with the crosshead speed of 0.5 mm/min.

2.3. Charpy impact testing

The impact test specimens were made from the 10 mm thick rolled alloy plates in the standard size. The impact tests were conducted using the JBDW-300Y testing machine with the test temperature ranged from −180 °C to 20 °C.

2.4. Samples characterization

The OLYMPUS GX51 metallographic microscope was used for microstructure characterization. JSM-6460LV scanning electron microscope (JEOL, Japan) was used for the tensile and impact test specimen fracture morphology characterization at the microscopic level. Digital camera DXM1200F (Nikon, Japan) was used to obtain the fracture macroscopic morphology of the impact test specimens at the macroscopic level.

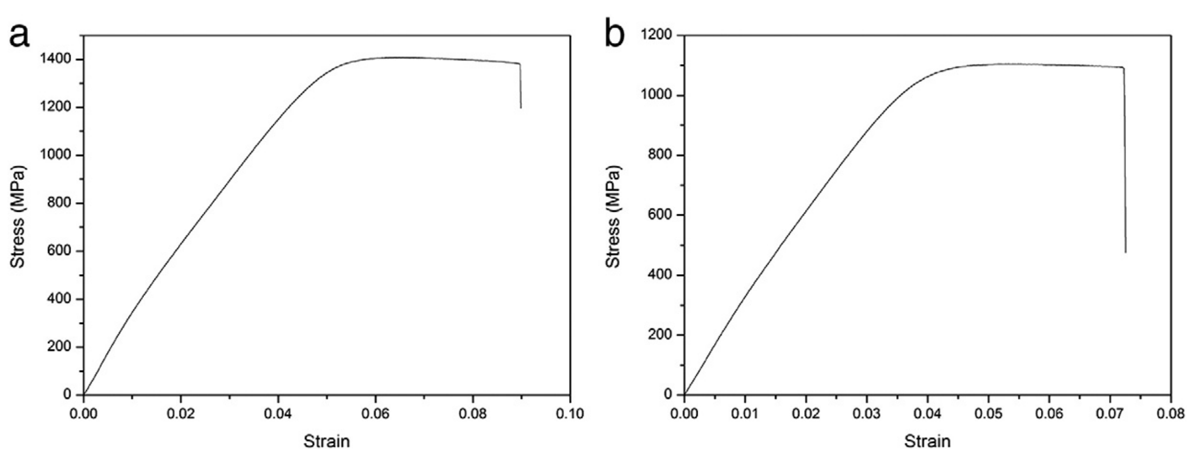

Fig. 3. Tensile stress–strain curve of (a) La-TZM alloy and (b) TZM alloy plates.

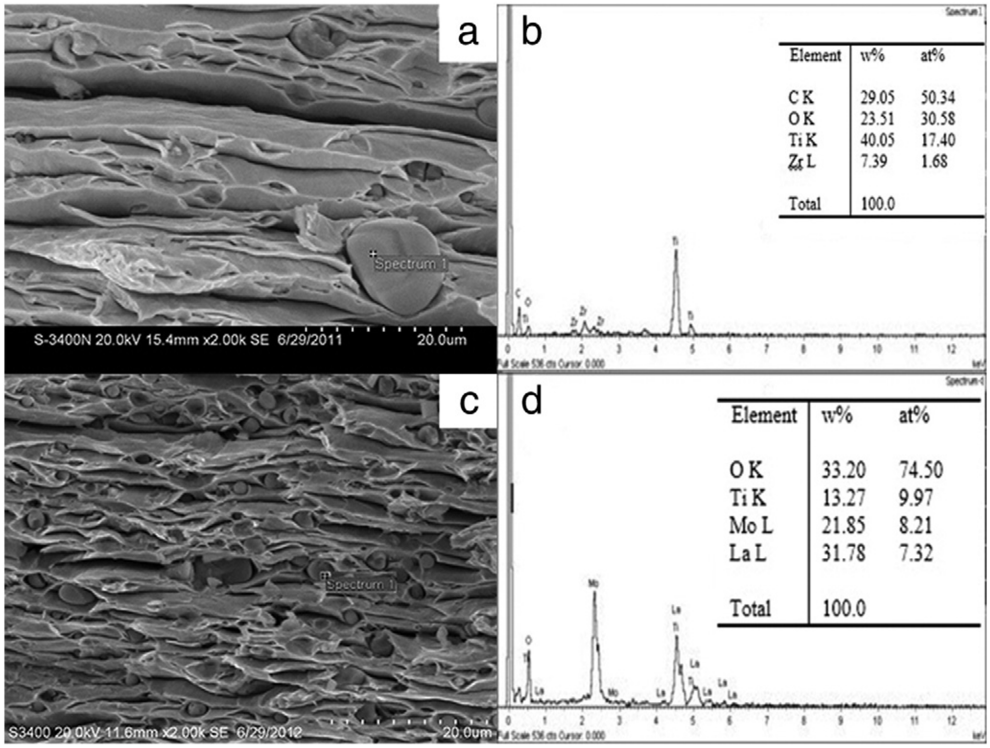

Fig. 4. The fracture morphology and secondary phase EDS spectra of (a) (b) TZM and (c) (d) La-TZM alloy plates.

3. Results and discussion

3.1. Cross-sectional metallography analysis

The structure of TZM and La-TZM alloys was observed in cross-section, using the metallography analysis. The optical micrographs are shown in Fig. 2.

The TZM and La-TZM alloy plates both show significant deformation texture after distinct plastic deformation. The secondary phase in the TZM alloy is coarse, asymmetrically distributed and segregated. The secondary phase of the La-TZM alloy is fine and uniform in both morphology and size. The volume and quantity of the secondary phase in La-TZM alloy are higher than that in TZM alloy, contributing the smaller grain size of La-TZM. In addition, the fiber texture in La-TZM is more tenuous and longer than that in the TZM alloy.

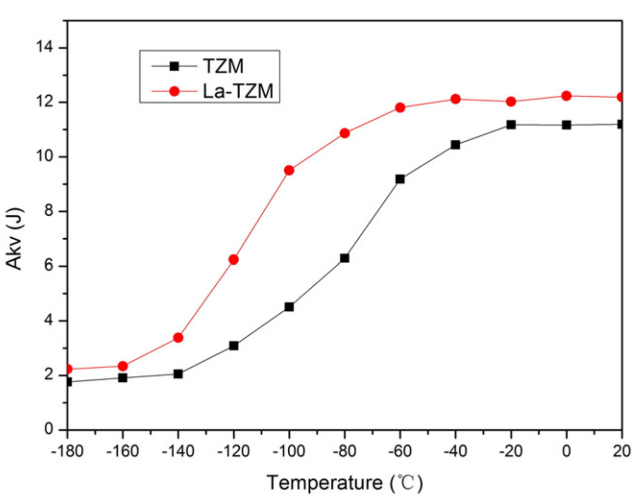

Fig. 5. Impact absorbed energy curves of the La-TZM and the traditional TZM alloys.

3.2. Tensile test results

3.2.1. Stress–strain curve analysis

The tensile stress–strain curves of the La-TZM and TZM alloys are shown in Fig. 3. From the stress–strain curves and the data in Table 2, the tensile strength of the TZM alloy manufactured using the same process is 1096 MPa, while the strength of the La-TZM alloy is 1405 MPa at room temperature. Both properties are superior compared with the literature values [13–16]. The tensile elongation of the TZM alloy is 7%, while the La-TZM is 9.3%. Therefore, lanthanum doping increases the tensile strength of the TZM alloy by 28.2%, and the elongation by 32.8%. In conclusion, lanthanum doping has significantly improved both the tensile strength and elongation.

3.2.2. Fracture SEM morphology

The SEM was used for observing the tensile fracture of the TZM and La-TZM alloy plate specimens, as shown in Fig. 4, along with the energy dispersive X-ray spectroscopy (EDS) results.

Fig. 4 exhibits obvious transverse cracks in the microscopic view of the tensile fracture. The interlining layer of the transverse cracks shows the lamellar structure with steps. In this area, the cracks distribute in a certain direction and they are step-shaped, which is characteristic of the intergranular fracture. Near the transverse cracks there is shape of tearing, characteristic of the crack growth regions. Around the tear cracks, there exist some light reflecting facets, which are cleavage planes. Therefore, the fracture region is a mixture of intergranular fracture and quasi-cleavage fracture.

As seen in the EDS image of Fig. 4, the secondary phase of TZM alloy mainly contains carbon, oxygen, titanium and zirconium, then that of La-TZM alloy mainly contains carbon, oxygen, titanium and lanthanum. And then, the morphology of the La-TZM alloy plate specimen fractures shows similar characteristics with TZM, while there are more secondary phase particles of the La-TZM alloy plates per unit area and the particles are smaller, mostly

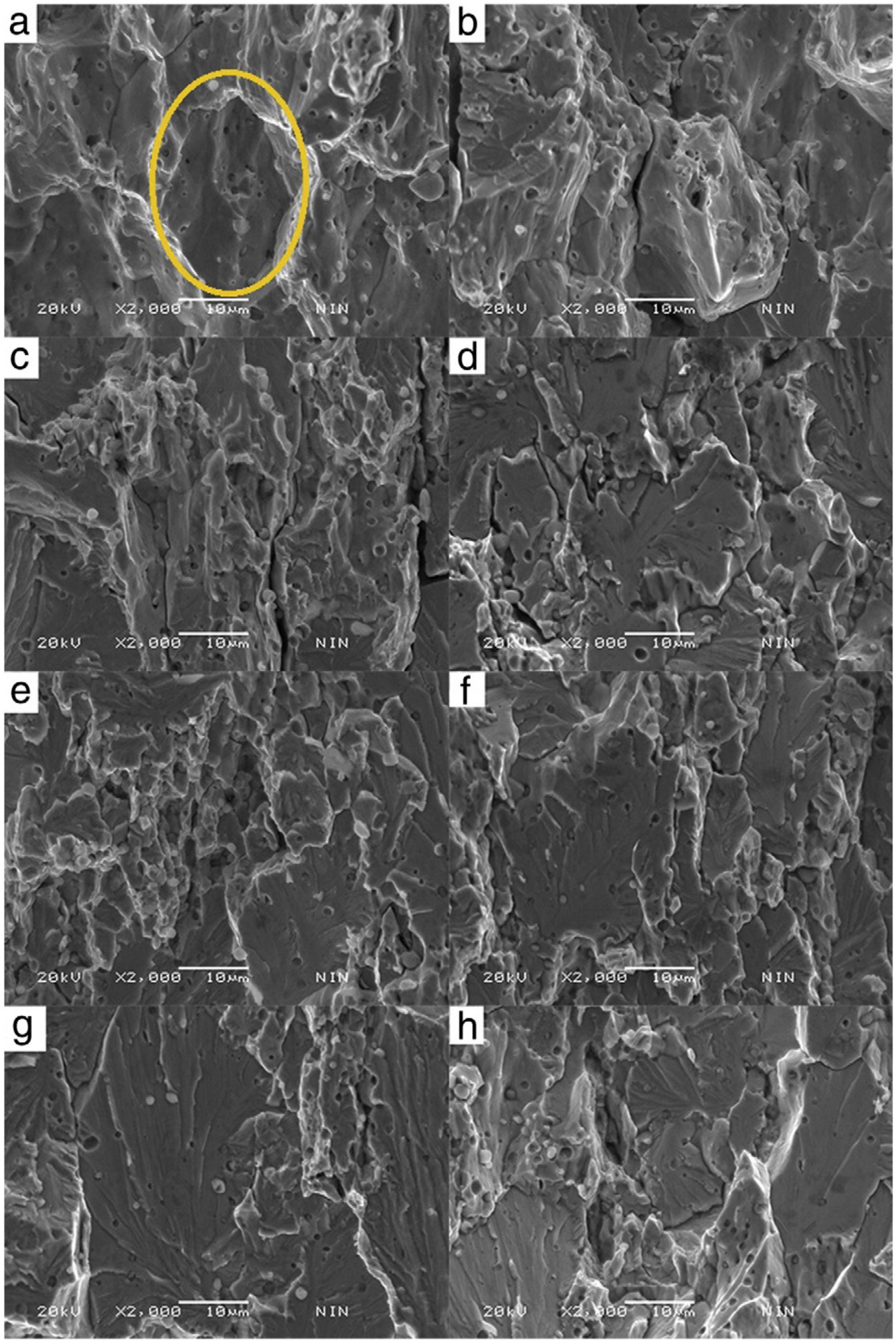

Fig. 6. Morphology of the La-TZM alloy fractured at different temperatures: (a) −40 °C; (b) −60 °C; (c) −80 °C; (d) −100 °C; (e) −120 °C; (f) −140 °C; (g) −160 °C; (h) −180 °C.

distributed around the grain boundaries. The secondary phase hinders the expanding of tearing crack. Near the transverse cracks, there are little cleavage facets and more step-shape structures, characteristic of the intergranular fracture. It supports some plastic deformation, which is why the La-TZM alloy plates have higher elongation than TZM.

The secondary phase pins in the grain boundaries and hinders the moving of the dislocation. Moreover, the smaller and uniform distributed secondary phase contributes to the segmentation of grain during the process of rolling, refining the grain size of alloy matrix. According to the theory of Hall–Petch [17], the smaller the grain size, the higher the tensile strength of alloy. This is why the La-TZM alloy has higher strength than the TZM alloy.

3.3. Charpy impact test results

3.3.1. Impact absorbing energy

Fig. 5 shows the impact absorbed energy curve of the La-TZM and traditional TZM alloys in the −180 °C to 20 °C temperature range.

As seen in Fig. 5, the impact absorbed energy curves of the La-TZM and traditional TZM alloys clearly show DBTT. With the decrease of temperature, the impact energy of both TZM and La-TZM decreases. This behavior indicates that a ductile-to-brittle transition happened in both alloys during the decrease of temperature. Based on the Charpy impact test, the ductile-to-brittle transition temperature of the La-TZM and traditional TZM alloys is determined as −120 °C and −80 °C, respectively. On the other hand, the impact absorbed energy of the La-TZM alloy is

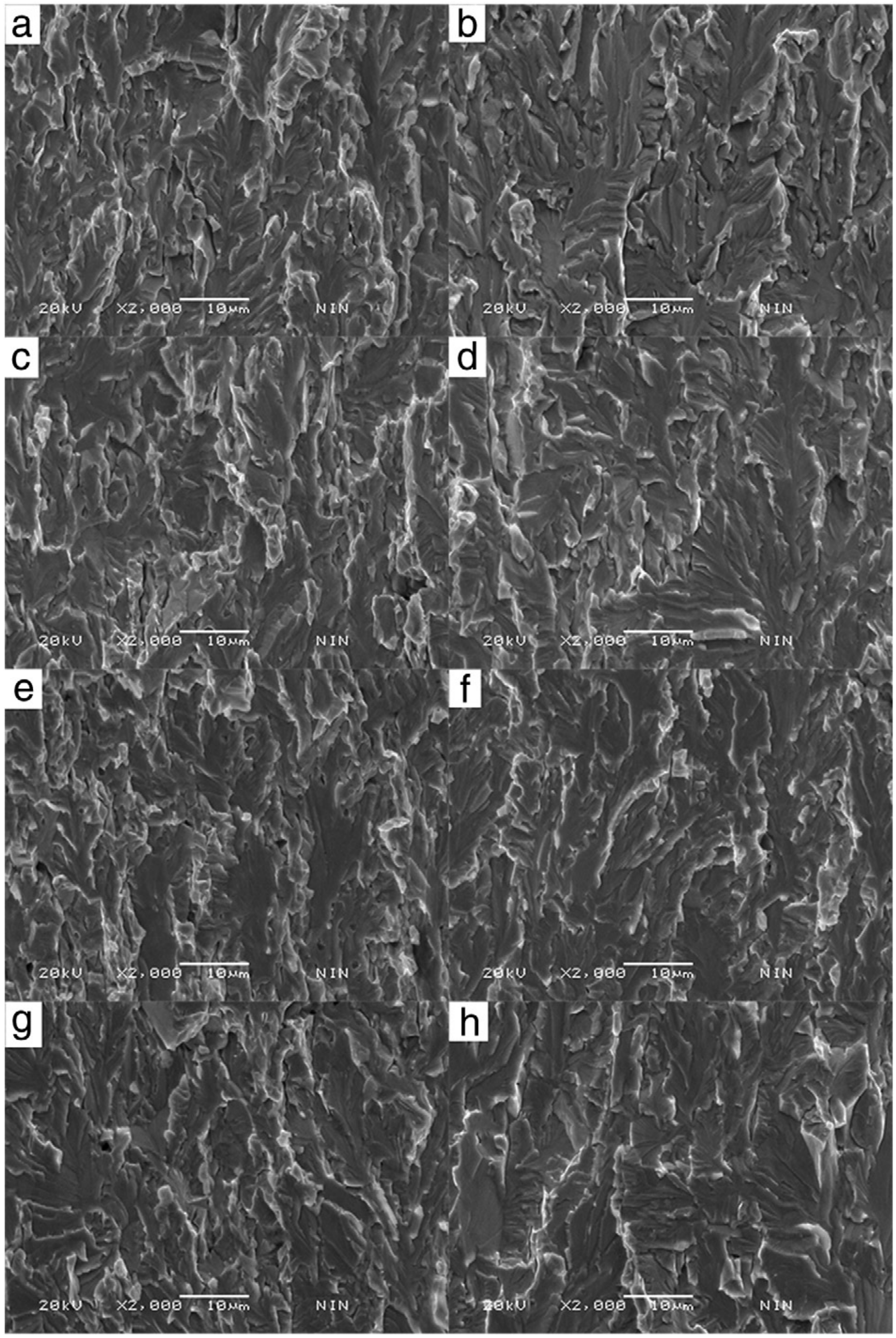

Fig. 7. Morphology of the TZM alloy fractured at different temperatures: (a) −20 °C; (b) −40 °C; (c) −60 °C; (d) −80 °C; (e) −100 °C; (f) −120 °C; (g) −140 °C; (h) −160 °C.

always higher than that of the TZM alloy for the same test temperature. These characteristics indicate that La doping can significantly improve the low temperature ductility of the TZM alloy with the DBTT reduction of 40 °C.

3.3.2. Fracture morphology

Figs. 6 and 7 show the fracture morphology of the La-TZM and TZM alloys fractured at different temperatures. As seen in Fig. 6, the La-TZM alloys fractured at −40 °C and −80 °C exhibit evident intergranular fracture. Dimples can be seen in Fig. 6(a)–(c), and microcracks along the grain boundaries indicate plastic fracture. The alloy starts to gradually exhibit brittle fracture with the temperature decrease. At −100 °C and −120 °C, transgranular crack surfaces appear with significant reduction of the number of dimples. A mixed fracture characteristic of intergranular and transgranular fracture can be seen in Fig. 6(d) and (e), which indicates that a change of fracture form has happened during the decrease of temperature. When the temperature is below −140 °C, dimples disappeared and the fracture surface is characterized by transgranular fracture, which is present in classic brittle fracture. This indicates that the fracture ductile-to-brittle transition of the La-TZM alloy starts between −100 °C and −120 °C.

For the TZM alloy fractured between −20 °C and −60 °C, ductile fracture with ductile step-shaped tears can be seen in Fig. 7(a)–(c). Transgranular fracture appears at −80 °C in Fig. 7(d), starting the ductile-to-brittle transition. With further temperature decrease, brittle fracture and transgranular cracks become more apparent. Therefore, the fracture ductile-to-brittle transition of the TZM alloy starts at −80 °C.

Table 3
The impact data and fracture modes of the La-TZM and TZM alloys at different temperatures.

Temperature (°C)	Akv (J)		Fracture mode	
	TZM	La-TZM	TZM	La-TZM
20	11.2	12.19	Ductile	Ductile
0	11.17	12.24	Ductile	Ductile
−20	11.18	12.03	Ductile	Ductile
−40	10.44	12.12	Ductile	Ductile
−60	9.19	11.81	Ductile	Ductile
−80	6.28	10.87	Ductile/brittle	Ductile
−100	4.51	9.51	Ductile/brittle	Ductile
−120	3.09	6.24	Brittle	Ductile/brittle
−140	2.05	3.38	Brittle	Ductile/brittle
−160	1.91	2.34	Brittle	Brittle
−180	1.76	2.23	Brittle	Brittle

As seen in Figs. 6 and 7, the secondary phase lanthanum oxide particles exist in both grains and grain boundaries of the La-TZM alloy, which hinder the transgranular fracture and the expanding of tearing crack. In addition, the lanthanum oxide particles refine the alloy grain size, which also improves toughness. Compared with the TZM alloy, the secondary phase in the La-TZM alloy promotes plasticity and reduces its ductile-to-brittle transition temperature. Table 3 sums up the impact energy data and fracture modes of the La-TZM and TZM alloys at different temperatures.

Combining the impact energy data and the fracture modes, one can draw a conclusion of the 40 °C DBTT decrease caused by the lanthanum doping of the TZM alloys. While the DBTT of the La-ZTM alloy is −120 °C, the DBTT of the traditional TZM alloy is −80 °C.

4. Conclusions

1) The strength and elongation of the La-TZM alloy plates exhibit better performance than the traditional TZM. For the same process conditions, the lanthanum doping has significantly improved tensile strength and elongation, which increased by 28.2% and 32.8%, respectively.
2) For these process conditions, the microstructure shows fiber texture. The La-TZM has higher density and smaller evenly distributed secondary phase, which is the main reason for the La-TZM alloy higher strength.
3) Compared with TZM, the secondary phase seen in the fracture surfaces of La-TZM is finer, and hinders the cracks spreading. That is why the La-TZM alloy plates have higher elongation than the TZM alloy plates.
4) By doping lanthanum, the ductile-to-brittle transition temperature of the TZM alloy was decreased by 40 °C to −120 °C. The secondary phase La particles refined the grain and hindered the fracture expansion across the grain in the Charpy impact fracture of the La-TZM alloy.

Acknowledgments

This work was supported by the Major Scientific and Technological Innovation Project of the Shaanxi Province (S2011ZK1087), the Science and Technology Innovation Fund Project of the Western Metal Materials Co., Ltd (XBCL-1-06), the Science and Technology Coordinating Innovative Engineering Project of the Shaanxi Province (2014KTCQ01-35) the workstation of postdoctoral scientific reserch in Jinduicheng Molybdenum Co., Ltd., the Innovation Team Foundation of Xi'an University of Architecture and Technology.

References

[1] G. Liu, G.J. Zhang, F. Jiang, X.D. Ding, Y.J. Sun, J. Sun, E. Ma, Nanostructured high-strength molybdenum alloys with unprecedented tensile ductility [J], Nat. Mater. 3544 (2013) 344–350.
[2] S. Majumdar, I.G. Sharma, Oxidation behavior of MoSi2 and Mo(Si, Al)2 coated Mo–0.5Ti–0.1Zr–0.02C alloy [J], Intermetallics 19 (2011) 541–545.
[3] S.P. Chakraborty, S. Banerjee, I.G. Sharma, A.K. Suri, Development of silicide coating over molybdenum based refractory alloy and its characterization [J], J. Nucl. Mater. 403 (2010) 152–159.
[4] S.P. Chakraborty, S. Banerjee, K. Singh, I.G. Sharma, A.K. Grover, A.K. Suri, Studies on the development of protective coating on TZM alloy and its subsequent characterization [J], J. Mater. Process. Technol. 207 (2008) 240–247.
[5] S. Majumdar, Formation of $MoSi_2$ and Al doped $MoSi_2$ coatings on molybdenum base TZM (Mo–0.5Ti–0.1Zr–0.02C) alloy [J], Surf. Coat. Technol. 206 (2012) 3393–3398.
[6] J.R. DiStefano, B.A. Pint, J.H. DeVan, Oxidation of refractory metals in air and low pressure oxygen gas [J], Int. J. Refract. Met. Hard Mater. 18 (2000) 237–243.
[7] S. Majumdar, R. Kapoor, S. Raveendra, H. Sinha, I. Samajdar, P. Bhargav, J.K. Chakravartty, I.G. Sharma, A.K. Suri, A study of hot deformation behavior and microstructural characterization of Mo-TZM alloy [J], J. Nucl. Mater. 385 (2009) 545–551.
[8] F. Yang, K.-S. Wang, P. Hu, H.-C. He, X.-Q. Kang, H. Wang, R.-Z. Liu, A.A. Volinsky, La doping effect on TZM alloy oxidation behavior [J], J. Alloys Compd. 593 (2014) 196–201.
[9] E. Ahmadi, M. Malekzadeh, S.K. Sadrnezhaad, Preparation of nanostructured high-temperature TZM alloy by mechanical alloying and sintering [J], J. Refract. Met. Hard Mater. 29 (2011) 141–145.
[10] H.J. Shi, L.S. Niu, C. Korn, G. Pluvinage, High temperature fatigue behaviour of TZM molybdenum alloy under mechanical and thermomechanical cyclic loads [J], J. Nucl. Mater. 278 (2000) 328–333.
[11] B.V. Cockeram, The mechanical properties and fracture mechanisms of wrought low carbon arc cast (LCAC), molybdenum–0.5pct titanium–0. 1pct zirconium (TZM), and oxide dispersion strengthened (ODS) molybdenum flat products [J], Mater. Sci. Eng. 418 (2006) 120–136.
[12] World wide web, Wikipedia [Online]. Ductility, http://en.wikipedia.org/wiki/Ductility (Last accessed on 9/3/2014).
[13] P. Hu, K.S. Wang, H.C. He, X.Q. Kang, H. Wang, P.Z. Wang, Appl. Mech. Mater. 320 (2013) 350–353.
[14] L. Wang, J. Sun, G. Liu, Y.J. Sun, G.J. Zhang, Influences of annealing temperature on microstructure and mechanical properties of Mo–La_2O_3 [J], Int. J. Refract. Met. Hard Mater. 29 (2011) 522–527.
[15] G.J. Zhang, X.H. Lin, R.H. Wang, G. Liu, J. Sun, Tensile properties and strengthening mechanisms of Mo–Si alloy [J], Int. J. Refract. Met. Hard Mater. 29 (2011) 608–613.
[16] G. Filacchioni, E. Casagrande, U. De Angelis, G. De Santis, D. Ferrara, Effects of strain rate on tensile properties of TZM and Mo–5%Re [J], J. Nucl. Mater. 307–311 (2002) 705–709.
[17] Takeshi Inoue, Yutak Hiraoka, Ei-ichi Sukedai, Masahiro Nagae, Jun Takada, Hardening behavior of dilute Mo–Ti alloys by two-step heat-treatment, Int. J. Refract. Met. Hard Mater. 25 (2007) 138–143.